

Contribution of rotational diffusion to pulsed field gradient diffusion measurements

Andrew J. Baldwin, John Christodoulou, Paul D. Barker, Christopher M. Dobson, and Guy Lippens

Citation: *J. Chem. Phys.* **127**, 114505 (2007); doi: 10.1063/1.2759211

View online: <http://dx.doi.org/10.1063/1.2759211>

View Table of Contents: <http://jcp.aip.org/resource/1/JCPSA6/v127/i11>

Published by the [American Institute of Physics](#).

Additional information on *J. Chem. Phys.*

Journal Homepage: <http://jcp.aip.org/>

Journal Information: http://jcp.aip.org/about/about_the_journal

Top downloads: http://jcp.aip.org/features/most_downloaded

Information for Authors: <http://jcp.aip.org/authors>

ADVERTISEMENT



AFM-RAMAN **BRUKER**

LEADING PERFORMANCE
WIDEST PRODUCT RANGE

www.bruker-axs.com

CLICK TO REQUEST INFO

Contribution of rotational diffusion to pulsed field gradient diffusion measurements

Andrew J. Baldwin, John Christodoulou, Paul D. Barker, and Christopher M. Dobson^{a)}
*Department of Chemistry, University of Cambridge, Lensfield Road, Cambridge CB2 1EW,
 United Kingdom*

Guy Lippens^{b)}
CNRS UMR8576, 59655 Villeneuve d'Ascq, France

(Received 9 May 2007; accepted 20 June 2007; published online 19 September 2007)

NMR diffusion experiments employing pulsed field gradients are well established as sensitive probes of the displacement of individual nuclear spins in a sample. Conventionally such measurements are used as a measure of translational diffusion, but here we demonstrate that under certain conditions rotational motion will contribute very significantly to the experimental data. This situation occurs when at least one spatial dimension of the species under study exceeds the root mean square displacement associated with translational diffusion, and leads to anomalously large apparent diffusion coefficients when conventional analytical procedures are employed. We show that in such a situation the effective diffusion coefficient is a function of the duration of the diffusion delay used, and that this dependence provides a means of characterizing the dimensions of the species under investigation. © 2007 American Institute of Physics. [DOI: 10.1063/1.2759211]

I. INTRODUCTION

NMR experiments employing pulsed field gradients (PFGs) have been used for many years to measure the diffusion coefficients of species in solution.¹ PFG NMR experiments directly measure the net displacement of nuclear spins during a defined delay, and such displacements can be related to the translational diffusion coefficients of the spins that give rise to the resonances in question.² As a noninvasive solution-state technique that yields information on the size of the species under study, this is a highly versatile experiment whose uses include probing ligand-receptor interactions,^{3,4} dissociation constants,⁵ membrane interactions,^{6,7} and the folding and aggregation of peptide and protein molecules.^{8–11}

The most common experimental approach to measuring such diffusion coefficients involves the use of a spin echo (SE),² and the resulting PFGSE experiments have been widely applied. By the end of the PFGSE pulse sequence, observable magnetization acquires a phase term, $\hat{I}_- e^{-i\alpha' \delta z}$, where δz is the net displacement of a spin during the experiment. The length scale is set by $\alpha' = G\gamma\delta$, the inverse of the pitch length generated by the pulsed gradient of field strength G and duration δ , where γ is the gyromagnetic ratio of the observed nucleus. To obtain an expression for the observed signal intensity of a sample, this term must be integrated over all spins in the system, where $P(\delta z)$ is a function that describes the probability of a given displacement occurring within the sample during the experiment. The diffusion weighted signal intensity, S_i , is then given by

$$S_i = \int_{-\infty}^{+\infty} \hat{I}_- P(\delta z) e^{-i\alpha' \delta z} d\delta z. \quad (1)$$

For a single species diffusing under Brownian motion for a time Δ , from the central limit theorem $P_{\text{trans}}(\delta z) = (1/2\sqrt{\pi D_T \Delta}) e^{-\delta z^2/4D_T \Delta}$, where the mean square displacement is related to the translational diffusion coefficient D_T , through $\langle \delta z^2 \rangle_{\text{trans}} = 2D_T \Delta$. Δ is the diffusion delay, during which magnetization is stored on the z axis, while the nuclear spins diffuse. Integration of Eq. (1) and setting $\alpha = G_{\text{max}} \gamma \delta$ yields the following equation, which relates the PFGSE signal intensity S_i , to the signal intensity obtained in the absence of the gradients, S_0 :

$$S_i = S_0 e^{-\alpha^2 D_T \Delta (G/G_{\text{max}})^2}. \quad (2)$$

This is the Stejskal-Tanner (ST) equation, and a plot of $\ln(S_i/S_0)/\alpha^2 \Delta$ against $(G/G_{\text{max}})^2$ yields a straight line of gradient $-D_T$,^{12,13} where G , δ , and Δ are experimental variables. When the duration of the applied gradients is considered in more detail, $\Delta = \Delta' - \delta/3$, where Δ' is the effective delay between the two applied gradients. This relationship will be explicitly assumed in this work.

Diffusion coefficients of proteins in the 10–30 kDa range, typical of the systems that are subject to studies by NMR spectroscopy, are on the order of $10^{-6} \text{ cm}^2 \text{ s}^{-1}$, with an R_H value of several nanometers.¹⁴ For an experimental diffusion delay of 50 ms, the corresponding root mean square displacement, $\sqrt{\langle \delta z^2 \rangle}$, is 4.4 μm and so is entirely dominated by translational diffusion. For larger molecular systems however, where the radius of hydration, R_H , is comparable with the net displacement due to translational diffusion, rotational diffusion will contribute to the displacement function $P(\delta z)$, and so contribute to the measured signal attenuation in the NMR experiment. By considering the effects of combined rotational and translational diffusion on $P(\delta z)$, through Eq. (1), we arrive in the present study at novel expressions [Eq. (11)] that describe the signal decay in NMR diffusion measurements. These expressions deviate from the form pre-

^{a)}Electronic mail: cmd44@cam.ac.uk

^{b)}Electronic mail: guy.lippens@univ-lille1.fr

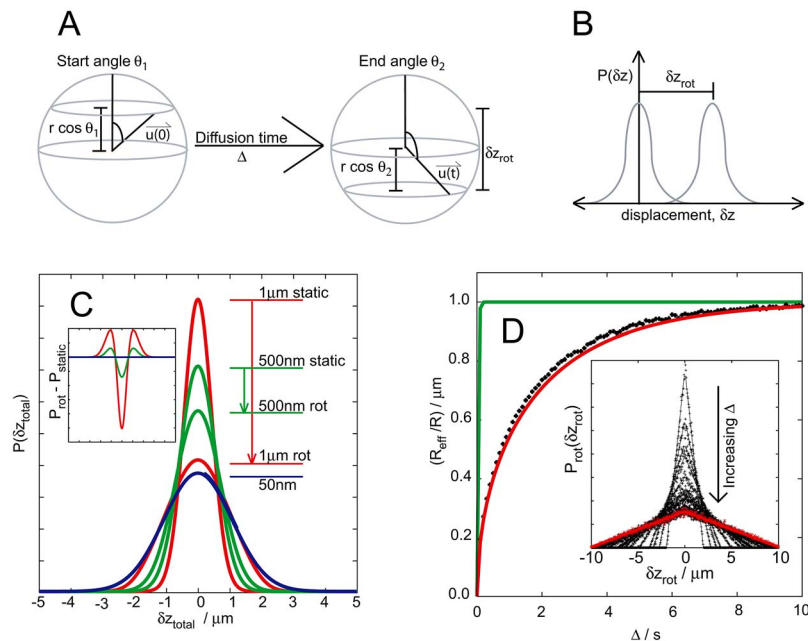


FIG. 1. (Color online) (a) Illustration of how rotational motion contributes to the displacement function of a point at distance r from the center of a sphere. (b) When this single rotation is considered in addition to a translational diffusion, it can be seen that it acts to shift the Gaussian translational displacement distribution by a constant distance δz_{rot} . (c) $P_{\text{total}}(\delta z)$ for spheres of radii $1 \mu\text{m}$ (red), 500 nm (green), and 50 nm (blue) for $\Delta = 100 \text{ ms}$ using the explicit form of Eq. (5) given in Appendix A. For each sphere, the distribution in the absence of rotation is shown, together with the distribution obtained in the limit of unrestricted diffusion. Remarkably, the displacement function for the rotating $1 \mu\text{m}$ sphere closely resembles that of the 50 nm sphere. The inset shows the difference between the displacement distribution functions in the static and rotating cases. For spheres of radii 50 nm , there is no difference between these two cases. For larger spheres, rotational motion promotes an increase in longer displacements at the expense of shorter displacements. (d) Inset: simulated $P_{\text{rot}}(\delta z_{\text{rot}})$ restricted distribution functions for rods of length $5 \mu\text{m}$ and radius 10 nm , calculated as described in Sec. IV. Distribution curves are drawn for Δ from 100 ms to 10 s (black) and compared to an unrestricted diffusion simulation (red). These values are fitted to Eq. (3) to obtain an effective radius, and plotted against Δ in the main figure (black points). These values are compared with the theoretical estimate for r_{eff} from Eq. (7) (red) and that for a rod of length $1 \mu\text{m}$ (green) which reaches its unrestricted diffusion limit much more rapidly than a $5 \mu\text{m}$ rod.

dicted in Eq. (2) and indicate that the apparent diffusion coefficient becomes a function of Δ . In this paper we describe the analysis that gives rise to this conclusion and consider its significance for the characterization of macromolecular dimensions.

II. RESULTS

A. Calculation of $P(\delta z)$ for rotating systems

Consider two spins placed within a hard sphere of radius r , one at the center and the other on the surface of the sphere. If during the diffusion time in a PFGSE experiment, the sphere rotates freely, then the measured displacement along the z axis for a spin on the surface of the sphere will differ from that of a spin at the center, as illustrated in Fig. 1(a). For the center of mass, the displacement will be given by $P_{\text{trans}}(\delta z) = (1/\sqrt{2\pi(\delta z^2)})e^{-\delta z^2/2(\delta z^2)}$. The function describing the behavior of a spin on the surface of the sphere requires further consideration. The effect of a single rotation from θ_1 to θ_2 , where the angles are defined with respect to the z axis, is to shift the translational distribution function by a constant value $\delta z_{\text{rot}} = r(\cos \theta_2 - \cos \theta_1)$, illustrated in Fig. 1(b). The width of this distribution function will not be affected by rotation, just the position of its maximum. For each displacement of the center of mass in the Brownian ensemble, the point on the sphere will undergo every possible rotation from every possible starting position, providing the time of the diffusion experiment Δ is large. Only the displacement along

the z axis is measured in the PFGSE experiment, so only the contribution of rotation to the displacement along the z axis need be considered in this context.

Defining \mathbf{u} as the vector connecting the origin and the point on the sphere in the laboratory reference frame as shown in Fig. 1(a), the rotational autocorrelation function $\langle \mathbf{u}(\mathbf{0}) \cdot \mathbf{u}(\mathbf{t}) \rangle$ will tend to zero in the limit of $t \rightarrow \infty$, indicating that θ_1 and θ_2 are completely independent. In this limit, the degeneracy of a given value of θ on the sphere is proportional to the circumference of the circle defined by the intersection of the sphere and the cone defined by θ . The probability of each starting angle is therefore $P(\theta_1) = \sin \theta_1 d\theta_1$ and each ending position $P(\theta_2) = \sin \theta_2 d\theta_2$. We can write the probability of a given $\theta_1 \rightarrow \theta_2$ as $P(\theta_1, \theta_2) = P(\theta_2 | \theta_1) \cdot P(\theta_1) = P(\theta_2) \cdot P(\theta_1)$. In this limit, we can calculate the rotational displacement probability function for a point on a sphere of radius r by imposing simply that the rotation leads to the required δz_{rot} ,

$$\begin{aligned}
 P_{\text{rot}}(\delta z_{\text{rot}}) &= \int_{\theta_1=0}^{\pi} \int_{\theta_2=0}^{\pi} \sin \theta_1 \sin \theta_2 \\
 &\quad \times \delta(r(\cos \theta_2 - \cos \theta_1) - \delta z_{\text{rot}}) d\theta_1 d\theta_2 \\
 &= \int_{-1}^1 \int_{-1}^1 \delta(r(u - v) - \delta z_{\text{rot}}) dudv \\
 &= \frac{1}{2r} \left(1 - \frac{|\delta z_{\text{rot}}|}{2r} \right), \tag{3}
 \end{aligned}$$

where we have integrated over the delta function. This triangular probability function can also be obtained by a simple Monte Carlo simulation, where we draw random start and end vectors on a unit sphere, and construct a histogram of δz_{rot} [Fig. 1(d), inset, red]. The average squared displacement of this distribution is given by

$$\langle \delta z_{\text{rot}}^2 \rangle = \frac{\int_{-2r}^{2r} \delta z^2 P_{\text{rot}}(\delta z) d\delta z}{\int_{-2r}^{2r} P_{\text{rot}}(\delta z) d\delta z} = \frac{2}{3} r^2. \quad (4)$$

The combined probability of a given displacement is therefore the convolution of the translational and rotational displacement probability distributions

$$\begin{aligned} P_{\text{total}}(\delta z) &= \int_{-\infty}^{\infty} P_{\text{rot}}(\tau) P_{\text{trans}}(\delta z - \tau) d\tau \\ &= \frac{1}{8\sqrt{\pi D_T \Delta}} \int_{\delta\tau=-\infty}^{\infty} \int_{\theta_1=0}^{\pi} \int_{\theta_2=0}^{\pi} \sin \theta_1 \sin \theta_2 \delta(r(\cos \theta_2 - \cos \theta_1) - \tau) e^{-(\delta z - \tau)^2/4D_T \Delta} d\theta_1 d\theta_2 d\tau \\ &= \frac{1}{8\sqrt{\pi D_T \Delta}} \int_{\theta_1=0}^{\pi} \int_{\theta_2=0}^{\pi} \sin \theta_1 \sin \theta_2 e^{-(\delta z - r(\cos \theta_2 - \cos \theta_1))^2/4D_T \Delta} d\theta_1 d\theta_2. \end{aligned} \quad (5)$$

This result shows, importantly, that the distribution function is no longer Gaussian as it was for purely translational diffusion. The integral form of the above equation can be expressed in a closed form in terms of error functions, the result of which is given in Appendix A. The mean squared displacement of a given spin undergoing both rotational and translational motion then becomes

$$\langle \delta z_{\text{total}}^2 \rangle = \frac{\int_{-\infty}^{\infty} \delta z^2 P_{\text{total}}(\delta z) d\delta z}{\int_{-\infty}^{\infty} P_{\text{total}}(\delta z) d\delta z} = \frac{2}{3} r^2 + 2D_T \Delta. \quad (6)$$

As both translational and rotational probability functions are independent, we obtain the linear sum of second moments. The displacement functions for spheres with radii of 1 μm , 500 nm, and 50 nm are shown in Fig. 1(c), which compares the normalized functions in the freely rotating and the static limits, and Fig. 1(c) (inset) shows the difference between the two. The distribution functions for the 50 nm spheres are essentially unaffected by the incorporation of rotational motion, but those for the 500 nm and 1 μm spheres are found to have a significant contribution from such motion. Remarkably, the 1 μm sphere has a displacement function with a root mean squared displacement similar to that of the 50 nm sphere. Figure 1(c) (inset) shows quantitatively that the probability of zero displacement is lowered, and that the probability of longer displacements increases. The displacement distributions when rotational effects become significant are no longer Gaussian, and thus rotational motion acts to increase the apparent diffusion of a nuclear spin.

1. The effect of restricted diffusion on $P(\delta z)$

For Brownian rotation over finite times, the rotational autocorrelation function $\langle \mathbf{u}(\mathbf{0}) \cdot \mathbf{u}(\mathbf{t}) \rangle$ can be expressed analytically^{15,16} as $\langle \cos \alpha \rangle = e^{-2D_R \Delta}$ where α is the angle subtended between the initial and final vectors, Δ is the diffusion delay, and D_R is the rotational diffusion coefficient. At finite times, the final angle θ_2 is no longer independent of the start angle θ_1 , as illustrated in Fig. 4 in Appendix B. Only when

the diffusion delay becomes large do we recover the previously described situation of independent starting and ending positions.

Although an analytical form of the displacement probability function in this regime of finite diffusion delays is not easily obtained, we can on the basis of a simple geometrical model (proof in Appendix B) calculate the average displacement due to rotational motion for the general case as

$$\langle \delta z_{\text{rot}}^2 \rangle = \frac{2}{3} r^2 (1 - e^{-2D_R \Delta}). \quad (7)$$

Interestingly, this average does not depend on a distribution function for the angle α separating the starting and ending orientations of the vector. Calculating the probability displacement function for combined rotational and translational motion in the limit $\langle \mathbf{u}(\mathbf{0}) \cdot \mathbf{u}(\mathbf{t}) \rangle = \langle \cos \alpha \rangle = e^{-2D_R \Delta}$ is complicated by the fact that $P_{\text{rot}}(\delta z_{\text{rot}})$ is a function of time in this regime. By comparing Eqs. (4) and (7) we can incorporate the time dependent rotation by using a reduced radius, $r_{\text{eff}} = r(1 - e^{-2D_R \Delta})^{1/2}$, and so θ_1 and θ_2 can still be considered to be independent.

We can simulate $P_{\text{rot}}(\delta z_{\text{rot}})$ for restricted diffusion using a Monte Carlo method, and by drawing rotation angles α that satisfy the distribution $\langle \cos \alpha \rangle = e^{-2D_R \Delta}$ a histogram of δz_{rot} can be calculated (see Sec. IV). The simulated distribution functions for $P_{\text{rot}}(\delta z_{\text{rot}})$ [Fig. 1(d) inset, black] show the same triangular distribution as for the case of unrestricted rotation, but the limits no longer span the interval $(-2r, 2r)$. Fitting the distributions to Eq. (3), we can estimate r_{eff} from the maximal displacement [Fig. 1(d), black points] and this estimate is in excellent agreement with the theoretical value for r_{eff} from Eq. (7) [Fig. 1(d), red]. Thus, the substitution of r for the reduced radius $r_{\text{eff}} = r(1 - \exp(-2D_R \Delta))$ into Eq. (5) provides a convenient method of estimating the effects of restricted diffusion. The restricted rotation factor $(1 - \exp(-2D_R \Delta))$ is shown in Fig. 2(a) for spheres (black

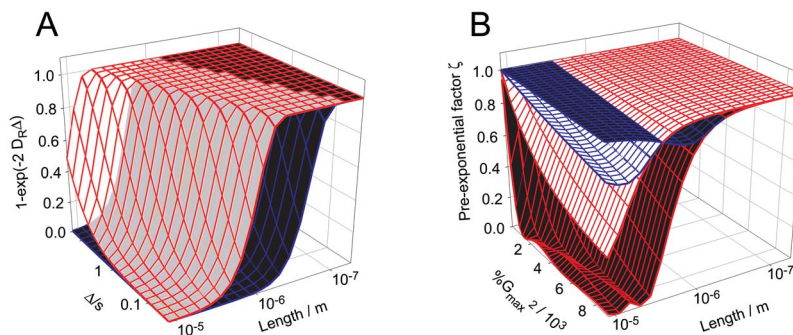


FIG. 2. (Color online) Rotational diffusion factors for spheres (black surfaces) and rods (white surfaces). (a) The restricted diffusion factor ($1 - e^{-2D_R\Delta}$) from Eq. (7). When this factor equals unity, rotations are unrestricted and θ_1 is independent of θ_2 . For short diffusion delays and larger particles, the factor is less than unity, and rotations are restricted. (b) The behavior of the preexponential factor ζ . When ζ equals unity, the ST equation is being obeyed, and rotational motion will not contribute to NMR diffusion measurements. The surfaces with red lines are calculated in the freely rotating limit, and the surfaces with blue lines are calculated for restricted diffusion, with $\Delta = 5$ s for both spheres and rods. Increasing Δ causes the surface in the restricted case to tend towards that of the freely rotating limit, and decreasing Δ causes it to tend to the static limit of unity. When $\zeta < 1$, i.e., where species are larger than $1 \mu\text{m}$, rotational motion will significantly contribute to the observed signal attenuation measured in a PFGSE experiment.

surface) and rods (white surface). For short times and large particles this factor deviates from unity, as rotation becomes restricted.

$P_{\text{total}}(\delta z)$ for any arbitrary rigid geometry can now be considered. All points on the object under investigation will have the same translational and rotational diffusion coefficients. Each point that defines the system is considered to be a single point on a sphere. Summing over the N point spheres that map out the geometry will then give the displacement function for the system as a whole such that $P_{\text{total}}^{\text{arb}}(\delta z) = 1/N \sum^N P_{\text{total}}(\delta z)$. A common and important geometry that is often of experimental interest is that of the rigid rod of length L . The rod here is considered as a collection of spheres of radii $-L/2$ to $L/2$. The displacement probability distribution is therefore given by $P_{\text{total}}^{\text{rod}}(\delta z) = 2/L \int_{-L/2}^{L/2} P_{\text{total}} dr$. The mean squared displacement can be calculated by integrating over Eq. (7),

$$\begin{aligned} \langle \delta z_{\text{total}}^2 \rangle_{\text{rod}} &= \frac{2}{L} \int_{-L/2}^{L/2} \langle \delta z_{\text{total}}^2 \rangle dr \\ &= \frac{1}{18} L^2 (1 - e^{-2D_R\Delta}) + 2D_T\Delta. \end{aligned} \quad (8)$$

The displacement due to translational diffusion will be constant for all points on the rod. Points near the center of the rod will experience less displacement due to a given rotation than a point near the end of the rod. The ratio of the rotational root mean square displacement of the end of a rod (a sphere of radius $L/2$) and the full length rod hence is

$$\frac{\langle \delta z_{\text{rot}}^2 \rangle_{\text{rod}}}{\langle \delta z_{\text{rot}}^2 \rangle_{\text{sphere}}} = \frac{\langle \delta z_{\text{rot}}^2 \rangle_{\text{rod}}}{\langle \delta z_{\text{rot}}^2 \rangle_{\text{rodend}}} = \frac{1}{3}. \quad (9)$$

This approach can be generalized to any arbitrary geometry. A treatment applied to spheroidal geometry is presented in Appendix C.

B. Derivation of NMR observables from rotational $P(\delta z)$ functions

1. Application to a point sphere

The effect of rotational diffusion and the resulting non-Gaussian displacement probability functions on the NMR experiment can be assessed by substituting the rotating $P(\delta z)$ expressions into Eq. (1) and integrating over the ensemble. For a point on a sphere, using Eq. (5) and noting $D_T\Delta$ is positive, the NMR intensity after a gradient echo, S_i , is related to the signal seen in the absence of a gradient echo, S_0 , by

$$\begin{aligned} S_i &= S_0 \int_{-\infty}^{+\infty} P_{\text{total}}(\delta z) e^{-i\alpha \delta z} d\delta z \\ &= \frac{S_0}{4} \int_{\theta_1=0}^{\pi} \int_{\theta_2=0}^{\pi} \sin(\theta_1) \sin(\theta_2) \\ &\quad \times e^{-D_T\alpha^2 - i r_{\text{eff}}\alpha(\cos\theta_2 - \cos\theta_1)} d\theta_1 d\theta_2. \end{aligned} \quad (10)$$

The imaginary part of the integral vanishes leading to the conclusion that size effects will not add gradient dependent phase terms to the expression. Evaluation of this integral yields the following important result:

$$S_i = S_0 \frac{\sin^2(\alpha r (1 - e^{-2D_R\Delta})^{1/2})}{\alpha^2 r^2 (1 - e^{-2D_R\Delta})} e^{-D_T\alpha^2\Delta}. \quad (11)$$

This function is the product of a Stejskal-Tanner factor, $\sigma(G, \delta, \Delta, L) = e^{-D_T\alpha^2\Delta}$, and a preexponential factor, a geometry dependent term $\zeta(G, \delta, \Delta, L)$. ζ is shown in Fig. 2(b) for spheres (black surfaces) in the freely rotating limit (red lines) and in the restricted diffusion limit for $\Delta = 5$ s (blue lines). As ζ deviates from unity, rotational effects will contribute to the PFGSE measurement. When the NMR signal is normalized to that acquired in the absence of gradients, S_0 , we obtain

$$\ln \frac{S_i}{S_0} = -D_T \alpha^2 \Delta + \ln \frac{\sin^2(\alpha r(1 - e^{-2D_R \Delta})^{1/2})}{\alpha^2 r^2 (1 - e^{-2D_R \Delta})}. \quad (12)$$

Two limiting cases are particularly interesting. When either the rotational diffusion coefficient or the diffusion delay are large, the effective radius of a sphere increases to its exact radius, leading to the following expression for the NMR data in the freely rotating limit:

$$\lim_{\Delta D_T \rightarrow \infty} S_i = S_0 \frac{\sin^2 \alpha r}{\alpha^2 r^2} e^{-D_T \alpha^2 \Delta}. \quad (13)$$

Here, the preexponential factor is no longer a function of the diffusion delay, but the ratio of the radius of the sphere and the length scale set by the pitch of the magnetization helix plays the dominant role. Where the product αr is small, the preexponential factor reduces to unity and Eq. (13) reduces to Eq. (2),

$$\lim_{\alpha r \rightarrow 0} S_i = S_0 e^{-D_T \alpha^2 \Delta}. \quad (14)$$

This expression reflects the fact that rotational motion will make no contribution to the PFGSE experiment when the species under consideration is small, and we recover the ST equation. In the limit where αr is small but not negligible, the signal intensity can be approximated by

$$T_i = 2S_0 \int_{r=0}^{L/2} \frac{\sin^2(\alpha r(1 - e^{-2D_R \Delta})^{1/2})}{\alpha^2 r^2 (1 - e^{-2D_R \Delta})} e^{-D_T \alpha^2 \Delta} dr$$

$$= S_0 \frac{\cos(\alpha L(1 - e^{-2D_R \Delta})^{1/2}) - 1 + \alpha L(1 - e^{-2D_R \Delta})^{1/2} \int_{t=0}^{\alpha L(1 - e^{-2D_R \Delta})^{1/2}} (\sin(t)/t) dt}{\frac{1}{2} \alpha^2 L(1 - e^{-2D_R \Delta})} e^{-D_T \alpha^2 \Delta}. \quad (16)$$

As in the case of the sphere, this expression takes the form of the product of a ST factor σ and a preexponential factor ζ , as shown in Fig. 2(b) (white surfaces) in the freely rotating limit (red lines) and in the restricted diffusion limit for $\Delta = 5$ s (blue lines). For the nonrotating case, when either $D_R \Delta$ or αr is small, ζ tends to unity and Eq. (16) reduces to Eq. (2). As a resonance from the center of a given rod will not undergo displacements due to rotational diffusion, the rod ζ function is seen to decay more slowly with field strength and length than is the case of a point from the center of mass as shown in Fig. 2. In the limit where $\alpha \rightarrow 0$, we can expand the trigonometric functions with their Taylor series, $T_0 = \lim_{\alpha L \rightarrow 0} T_i = LS_0$, yielding

$$\ln \frac{T_i}{T_0} = -D_T^{\text{rod}} \Delta \alpha^2 + \ln \frac{\cos(\alpha L(1 - e^{-2D_R \Delta})^{1/2}) - 1 + \alpha L(1 - e^{-2D_R \Delta})^{1/2} \int_{t=0}^{\alpha L(1 - e^{-2D_R \Delta})^{1/2}} (\sin(t)/t) dt}{\frac{1}{2} \alpha^2 L^2 (1 - e^{-2D_R \Delta})}. \quad (17)$$

In the limit where αL is small, we can expand this expression to give

$$\lim_{\alpha r \rightarrow 0} \ln \frac{T_i}{T_0} = \left(-D_T^{\text{rod}} - \frac{L^2(1 - e^{-2D_R \Delta})}{36\Delta} \right) \Delta \alpha^2 = -D_{\text{eff}}^{\text{rod}} \alpha^2 \Delta, \quad (18)$$

$$D_{\text{eff}}^{\text{rod}} = D_T^{\text{rod}} + \frac{L^2(1 - e^{-2D_R \Delta})}{36\Delta},$$

and D_{eff} is a function of Δ when $L^2/36\Delta > D_T^{\text{rod}}$. The decay of signal intensity again is expected to follow a single expo-

$$\lim_{\alpha r \rightarrow 0} \ln \frac{S_i}{S_0} = \left(-D_T - \frac{r^2(1 - e^{-2D_R \Delta})}{3\Delta} \right) \alpha^2 \Delta$$

$$= -D_{\text{eff}}^{\text{sphere}} \alpha^2 \Delta, \quad (15)$$

$$D_{\text{eff}}^{\text{sphere}} = D_T + \frac{r^2(1 - e^{-2D_R \Delta})}{3\Delta}.$$

Thus intensity will decay with a single exponential function, with the *effective diffusion coefficient*, D_{eff} , not simply the translational diffusion coefficient as predicted by the ST equation, but a function of Δ when $(r^2/3\Delta) > D_T$. The decay deviates from monoexponential with a term in $\alpha^4 R^4$. Experimentally therefore, monoexponential decays are predicted with D_{eff} expected to be larger for shorter values of Δ as spins at a large distance from the center of mass will appear to diffuse much more quickly than in the case when diffusion depends solely on the translational motion of the particle under consideration. A similar result can be derived for rigid rods as we now show.

2. Application to a rigid rod

By integrating Eq. (11) we arrive at the following result for the total NMR signal intensity from a rigid rod of length L :

nential function, with curvature developing with a term in $\alpha^4 R^4$.

C. Calculation of NMR diffusion data

Using theoretical models for D_T and D_R we are now in a position to calculate NMR diffusion data under conditions where these models are valid. Calculated friction factors, f , are related to diffusion coefficients through the Einstein relation $D = k_B T / f$, where T is the thermodynamic temperature and k_B is the Boltzmann constant. Friction factors derived

TABLE I. Translational, f_T , and rotational, f_R , friction factors, preexponential factors ζ , and limiting preexponential functions $\lim_{\alpha r \rightarrow 0} \zeta$ for idealized geometries. η is the viscosity, r is the radius, and L is the rod length.

Geometry	f_T	f_R	ζ	$\lim_{\alpha r \rightarrow 0} \zeta$
Sphere	$6\pi\eta r$	$8\pi\eta r^3$	$\sin^2 \alpha r / \alpha^2 r^2$	1
Rod	$3\pi\eta L(1/\ln(L/r) - 0.3)^a$	$\pi\eta L^3/3 \ln(L/r)^b$	$[\cos(\alpha L) - 1 + \alpha L \int_{t=0}^{\alpha L} (\sin(t)/t) dt] / \frac{1}{2}\alpha^2 L$	L

^aReference 17.

^bReference 18.

from theory for hard spheres, rigid rods, and spheroids, and the derived ζ functions for the appropriate geometries are summarized in Table I, using the parameters stated in Sec. IV.

Simulated NMR intensity data, scaled as $1/\alpha^2 \Delta \ln S_i/S_0$ with $\alpha = G_{\max} \gamma \delta$, for rods of 2.4 μm in length are shown in Fig. 3(a), plotted against the applied field gradient given as the percentage of the maximum gradient G_{\max} , the experimental parameter that is explicitly varied during typical experiments. When plotted in this way, all the data will lie on a straight line of gradient $-D_T$ if the ST equation is obeyed, a situation observed in the nonrotating limit for rigid rods (Fig. 3, green lines). When a combination of rotational and translational diffusion is considered, the ST equation is no longer sufficient and the data no longer fall on a single line. D_{eff} can be taken as the slope of each plot [Fig. 3(b)]. This slope is found to be a function of the diffusion delay when rotational effects are incorporated in the model.

Diffusion data with Δ of 100 ms, a typical delay employed in PFGSE measurements, are shown in Fig. 3(c). When rotation is neglected, the diffusion data scale as expected (green surface), with the slope decreasing with the length. When rotations in the freely rotating limit are considered (blue surface), for rods of length greater than $\sim 1 \mu\text{m}$, the slope increases as the rotational term starts to dominate and D_{eff} increases with rod length; the value of D_{eff} as a

function of rod length and Δ is shown in Fig. 3(d). For longer rods, and shorter diffusion delays, D_{eff} is significantly larger than D_T . As the displacement due to translational motion increases with time, at large values of Δ , the ST factor dominates and D_{eff} tends to D_T . This is equivalent to noting that for larger Δ , the NMR signals from the rapidly diffusing rod ends will have been significantly attenuated and so the only observable signals will be from the center of the rod. In addition, when the system under study has a heterogeneous size distribution, account for this can be taken by multiplying Eq. (16) by a size distribution function and then summing over the distribution. This procedure is described in Appendix D.

III. DISCUSSION

NMR signals originating from even large macromolecular structures can be observed using conventional solution-state experiments when regions of the structure have sufficient mobility to average out local inhomogeneities and residual dipolar interactions. Such “motional narrowing” leads to narrow solution-state NMR linewidths that are typically observed from these mobile regions at chemical shifts that are approximately those expected for a random coil. One example of such a case is that of amyloid fibrils for which NMR signals from flexible noncore regions can be

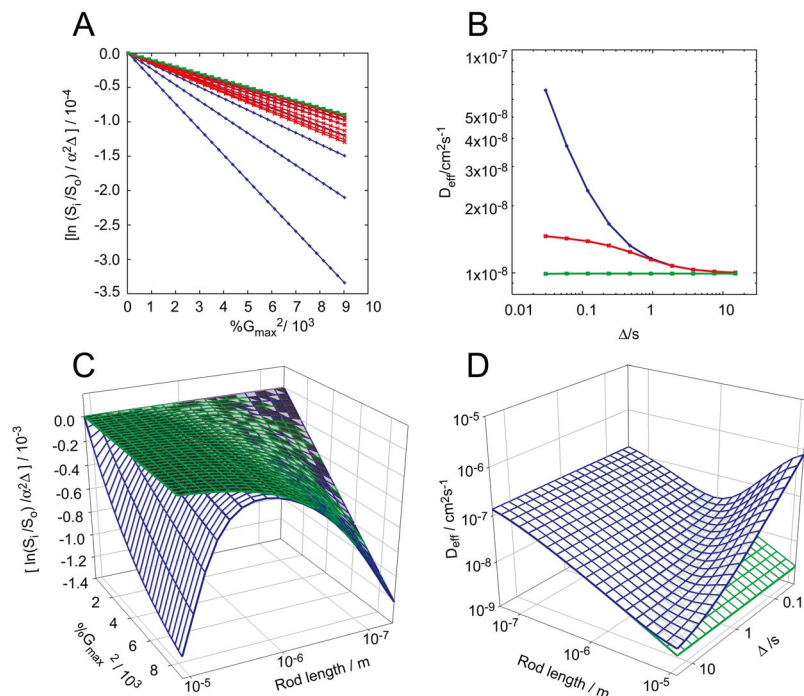


FIG. 3. (Color online) Simulated NMR intensity data and D_{eff} for rigid rods. (a) Intensity data as a function of $\%G_{\max}^2$ for rods of length 2.4 μm , and Δ ranging from 30 ms to 15 s in the freely rotating limit (blue lines), under restricted rotation (red lines), and in the static limit (green lines). As plotted, the gradient of the intensity data is independent of Δ in the static regime. (b) D_{eff} against Δ obtained from taking the gradients of the plots in (a). D_{eff} is a function of the experimental diffusion delay. (c) Simulated data for $\Delta = 100$ ms of increasing length in the freely rotating limit (blue surface) and static limit (green surface). (d) Variation of effective diffusion coefficients with rod length and Δ . As the rod length exceeds 1 μm , D_{eff} in the freely rotating limit is significantly larger than that expected from the effects of translational diffusion alone.

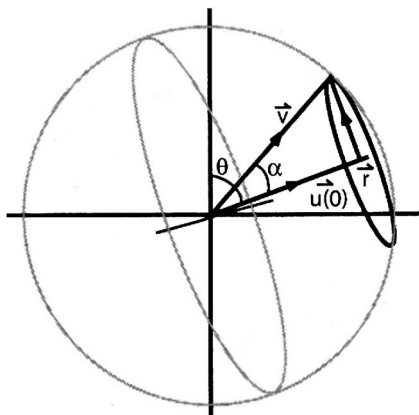


FIG. 4. The vectors that define the rotation of a point on the surface of a sphere.

observed.^{19–21} While characterizing these regions using NMR pulsed field gradients, we observed that measured apparent diffusion coefficients of the fibrils were comparable to those of monomeric protein molecules, rather than to a large molecular assembly.

In the light of this observation we have explored theoretically the contribution that rotational diffusion of large assemblies can make to NMR diffusion measurements. Rotational diffusion can lead to displacements that are comparable to, or even larger than, those due to translational diffusion, and D_{eff} can be seen to be a function of Δ and α . This variance is qualitatively similar to the case of restricted diffusion, where a similar $\text{sinc}^2 \alpha R$ function²² to that in Eq. (13) is observed, although it has a different origin. By observing the variance of D_{eff} with Δ and α , the results suggest that dimensions of the macromolecular species under study can be determined. In accord with this conclusion, application of this approach to calculate length distributions in solutions containing protein amyloid fibrils has, for example, has generated results that agree well with those derived from atomic force microscopy and transmission electron microscopy measurements.²³

We can therefore conclude that NMR diffusion measurements coupled with the theory described in this work can provide a powerful method for probing noninvasively the dimensions of large molecular assemblies in solution, and provide a means for observing changes in such systems as a function of time and solution conditions. We therefore believe that this strategy should be of considerable value in the context of studies of macromolecular structure and assembly.

IV. METHODS

A. Calculations

The model was coded into C++ using functions from the GNU Scientific Library.²⁴ Plots were prepared using GNUPLOT 4.0 with scripts generated by the program, and ILLUSTRATOR 10. The program, including routines for fitting experimental data to the model, is available on request. All calculations were performed assuming $\eta=0.1$ cP, $T=300$ K, and $\delta=5.4$ ms. On a Bruker DRX-500, using sinusoidal bi-

polar gradients, $G_{\text{max}}=32$ G cm⁻¹ and so this value was used in all calculations.

B. Monte Carlo simulations

The triangular rotational distribution functions were simulated using a Monte Carlo method. By drawing angles with a sinusoidal distribution between 0 and 2β , with β defined by $0.5(1+\cos\beta)=\exp(-2D_R\Delta)$, histograms of δz_{rot}^2 were generated using the theoretical models for D_R defined in Table I. Δ was varied from 100 ms to 10 s with typically 60 000 runs for each [Fig. 1(d), inset]. The triangular distributions in the freely rotating limit were obtained by drawing start and end angles at random, on the surface of a unit sphere.

ACKNOWLEDGMENTS

We thank Giorgio Favrin and Shang-Te Danny Hsu for helpful discussions and the MRC, the Wellcome and Leverhulme Trusts, and the Cambridge Nanoscience Centre for financial support of this work.

APPENDIX A: EXPLICIT DISPLACEMENT FUNCTIONS

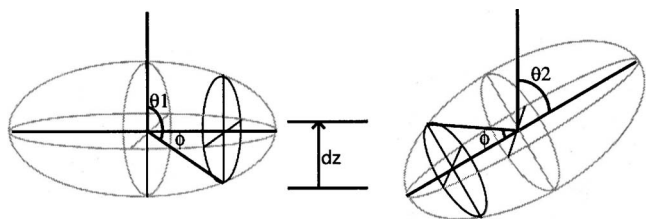
Where $b=2D_T\Delta$, the freely rotating displacement function from Eq. (5) is given by Eq. (A1), for a point a distance a from the surface of a sphere, shown graphically in Fig. 1(c),

$$\begin{aligned}
 P(z) &= \int_{\theta_1=0}^{\pi} \int_{\theta_2=0}^{\pi} \frac{1}{4\sqrt{b}\pi} \sin\theta_1 \sin\theta_2 e^{-(z-a(\cos\theta_2-\cos\theta_1))^2/b} \\
 &= \frac{1}{8a^2} \left(\frac{\sqrt{b}}{\sqrt{\pi}} (e^{-(z-2a)^2/b} + e^{-(z+2a)^2/b} - 2e^{-z^2/b}) \right. \\
 &\quad \left. + (2a-z)\text{erf}\left(\frac{2a-z}{\sqrt{b}}\right) - 2z\text{erf}\left(\frac{z}{\sqrt{b}}\right) \right. \\
 &\quad \left. + (z+2a)\text{erf}\left(\frac{2a+z}{\sqrt{b}}\right) \right). \tag{A1}
 \end{aligned}$$

APPENDIX B: EFFECTS OF RESTRICTED ROTATION ON A SPHERE

Proof of Eq. (7) involves calculating the displacement due to rotation of a point on a sphere undergoing Brownian diffusion.

The vector \mathbf{u} is initially at an angle θ to the z axis. After a time Δ , it has rotated through α . The end vector is given by $\mathbf{u}(\mathbf{t})$ where angle ψ sweeps through the cone defined by $\mathbf{u}(\mathbf{0})$ and α , as shown in Fig. 4,

FIG. 5. The effect of sets of equivalent rotations on δz for ellipsoids.

$$\mathbf{u}(\mathbf{0}) = \cos \theta \mathbf{e}_z + \sin \theta \mathbf{e}_x,$$

$$\mathbf{u}(\mathbf{0})_{\perp} = \sin \theta \mathbf{e}_z - \cos \theta \mathbf{e}_x, \quad (\text{B1})$$

$$\mathbf{v} = \cos(\theta - \alpha) \mathbf{e}_z + \sin(\theta - \alpha) \mathbf{e}_x = \cos \alpha \mathbf{u}(\mathbf{0}) + \sin \alpha \mathbf{u}(\mathbf{0})_{\perp}.$$

Rotating \mathbf{v} by ψ about $\mathbf{u}(\mathbf{0})$ gives $\mathbf{u}(t) = \cos \alpha \mathbf{u}(\mathbf{0}) + \sin \alpha (\cos \psi \mathbf{u}(\mathbf{0})_{\perp} + \sin \psi \bar{\mathbf{e}}_y)$, the position on the surface of the sphere at time t . Calculating the square displacement along the z axis, and averaging over the cone give

$$\begin{aligned} &= \frac{1}{r^2} \int_{\psi=0}^{\pi} (z(t) - z(0))^2 d\psi \\ &= \int_{\psi=0}^{\pi} (\cos \alpha \cos \theta + \cos \psi \sin \alpha \sin \theta - \cos \theta)^2 d\psi \\ &= \cos^2 \theta (\cos \alpha - 1)^2 + \frac{1}{2} \sin^2 \alpha \sin^2 \theta. \end{aligned} \quad (\text{B2})$$

Averaging over all start positions gives

$$\begin{aligned} \frac{\langle z_{\text{rot}}^2 \rangle}{r^2} &= \frac{\int_{\theta=0}^{\pi} \sin \theta (\cos^2 \theta (\cos \alpha - 1)^2 + \frac{1}{2} \sin^2 \alpha \sin^2 \theta) d\theta}{\int_{\theta=0}^{\pi} \sin \theta d\theta} \\ &= \frac{2}{3} (1 - \cos \alpha) = \frac{2}{3} (1 - e^{-2D_R \Delta}). \end{aligned} \quad (\text{B3})$$

This result is Eq. (7). In the limit $t \rightarrow \infty$, this expression reduces to Eq. (4). By comparing Eq. (7) to Eq. (4) we can make the approximation $r_{\text{eff}} = r \sqrt{1 - e^{-2D_R \Delta}}$. At shorter diffusion times, the displacement caused by rotation is reduced as a result of the finite time required for Brownian rotational diffusion.

APPENDIX C: DISPLACEMENT FUNCTION FOR SPHEROIDS

An ellipsoid is defined by the equation $1 = x^2/a^2 + y^2/b^2 + z^2/c^2$, and the spheroid is the case where $b=c=na$. The case where $n < 1$ is therefore prolate, and where $n > 1$, the spheroid is oblate. Considering points along the x, y plane, all points are a distance $r = \sqrt{z^2 + x^2} = \sqrt{n^2 a^2 + z^2 (1 - n^2)}$ from the center of mass. Each distance should be weighted by the circumference of the circle defined by constant ϕ as shown in Fig. 5, and so the degeneracy is $2\pi \sqrt{n^2(a^2 - z^2)}$. Using Eq. (5), substituting $r = \sqrt{n^2 a^2 + z^2 (1 - n^2)}$,

$$P_{\text{total}}^{\text{spheroid}}(\delta z) = \frac{\int_{z=0}^a \sqrt{n^2(a^2 - z^2)} P_{\text{total}} dz}{\int_{z=0}^a \sqrt{n^2(a^2 - z^2)} dz}. \quad (\text{C1})$$

The mean squared displacement is then given by

$$\begin{aligned} \langle \delta z_{\text{rot}}^2 \rangle_{\text{spheroid}} &= \frac{2 \int_0^a \sqrt{n^2(a^2 - z^2)} (n^2 a^2 + z^2 (1 - n^2)) dz}{3 \int_0^a \sqrt{n^2(a^2 - z^2)} dz} \\ &= \frac{1}{6} (3a^2 n^2 + a^2), \end{aligned} \quad (\text{C2})$$

which in the limit where $n \rightarrow 1$, reduces to Eq. (6), as expected.

APPENDIX D: EFFECTS OF A POPULATION DISTRIBUTION ON NMR OBSERVABLES

In a heterogeneous sample, we can expect a distribution of the lengths of rods or the diameters of spheres. Certainly in a solution of amyloid fibrils, the lengths are observed to vary over several orders of magnitude. Account must be taken of this variation if the model is used to analyze experimental data. In all cases, with a prefactor $\zeta(l, G, \delta, \Delta)$, and the Stejskal-Tanner factor $\sigma(G, \delta, \Delta, l)$, where the sample has a distribution of lengths given by the function $C(l)$, the PFGSE signal intensity decay is given by

$$\ln \frac{S_i}{S_0} = \ln \frac{\sum_{l=0}^{\infty} C(l) \zeta(G, \delta, \Delta, l) \sigma(G, \delta, \Delta, l)}{\sum_{l=0}^{\infty} C(l) \lim_{G \rightarrow 0} \zeta(l)}. \quad (\text{D1})$$

- ¹H. C. Torrey, Phys. Rev. **104**, 563 (1956).
- ²A. Dehner and H. Kessler, ChemBioChem **6**, 1550 (2005).
- ³X. R. Qin, Y. Ishizuka, J. S. Lomas, T. Tezuka, and H. Nakanishi, Magn. Reson. Chem. **40**, 595 (2002).
- ⁴H. Ponstingl and G. Otting, J. Biomol. NMR **9**, 441 (1997).
- ⁵C. Y. Mayzel and Y. Cohen, J. Chem. Soc., Chem. Commun. 1994, 1901.
- ⁶K. Bleicher, M. Lin, M. Shapiro, and J. Wareing, J. Org. Chem. **63**, 8486 (1998).
- ⁷J. J. Chou, J. L. Baber, and A. Bax, J. Biomol. NMR **29**, 299 (2004).
- ⁸A. Dehner, E. Planker, G. Gemmecker, Q. Broxterman, W. Bisson, F. Formaggio, M. Crisma, C. Toniolo, and H. Kessler, J. Am. Chem. Soc. **123**, 6678 (2001).
- ⁹X. Chang, D. Keller, S. I. O'Donoghue, and J. J. Led, FEBS Lett. **515**, 165 (2002).
- ¹⁰J. A. Jones, D. K. Wilkins, L. J. Smith, and C. M. Dobson, J. Biomol. NMR **10**, 199 (1997).
- ¹¹J. Balbach, J. Am. Chem. Soc. **122**, 5887 (2000).
- ¹²E. O. Stejskal and J. E. Tanner, J. Chem. Phys. **42**, 288 (1965).
- ¹³J. E. Tanner, J. Chem. Phys. **52**, 2523 (1970).
- ¹⁴D. K. Wilkins, C. M. Dobson, and M. Gross, Eur. J. Biochem. **267**, 2609 (2000).
- ¹⁵F. Perrin, J. Phys. Radium **7**, 1 (1936).
- ¹⁶Y.-G. Tao, W. K. den Otter, J. T. Padding, J. K. G. Dhont, and W. J. Briels, J. Chem. Phys. **122**, 244903 (2005).
- ¹⁷H. Yamakawa and G. Tanaka, J. Chem. Phys. **57**, 1537 (1972).
- ¹⁸S. Broersma, J. Chem. Phys. **32**, 1626 (1960).
- ¹⁹A. J. Baldwin, R. Bader, J. Christodoulou, C. E. MacPhee, C. M. Dobson, and P. D. Barker, J. Am. Chem. Soc. **128**, 2162 (2006).
- ²⁰A. Sillen, A. Leroy, J. M. Wieruszkeski, A. Loyens, J. C. Beauvillain, L. Buee, I. Landrieu, and G. Lippens, ChemBioChem **6**, 1849 (2005).
- ²¹A. Siemer, A. Arnold, C. Ritter, T. Westfeld, M. Ernst, R. Riek, and B. Meier, J. Am. Chem. Soc. **128**, 13224 (2006).
- ²²J. E. Tanner and E. O. Stejskal, J. Chem. Phys. **49**, 1768 (1968).
- ²³A. Baldwin, S. J. Anthony-Cahill, J. Christodoulou, G. Lippens, P. D. Barker, and C. M. Dobson, Angew. Chem., Int. Ed. (submitted).
- ²⁴<http://www.gnu.org/software/gsl/>